

First results of the *XI* Groups Project: Studying an unbiased sample of galaxy groups

Jesper Rasmussen,^{1*} Trevor J. Ponman,¹ John S. Mulchaey,² Trevor A. Miles¹ and Somak Raychaudhury¹

¹*School of Physics and Astronomy, University of Birmingham, Edgbaston, Birmingham B15 2TT*

²*Observatories of the Carnegie Institution, 813 Santa Barbara Street, Pasadena, California, USA*

ABSTRACT

X-ray observations of hot, intergalactic gas in galaxy groups provide a useful means of characterizing the global properties of groups. However, X-ray studies of large group samples have typically involved very shallow X-ray exposures or have been based on rather heterogeneous samples. Here we present the first results of the *XI* (XMM/IMACS) Groups Project, a study targeting, for the first time, a redshift-selected, statistically unbiased sample of galaxy groups using deep X-ray data. Combining this with radio observations of cold gas and optical imaging and spectroscopy of the galaxy population, the project aims to advance the understanding of how the properties and dynamics of group galaxies relate to global group properties. Here, X-ray and optical data of the first four galaxy groups observed as part of the project are presented. In two of the groups we detect diffuse emission with a luminosity of $L_X \approx 10^{41}$ erg s⁻¹, among the lowest found for any X-ray detected group thus far, with a comparable upper limit for the other two. Compared to typical X-ray selected groups of similar velocity dispersion, these four systems are all surprisingly X-ray faint. We discuss possible explanations for the lack of significant X-ray emission in the groups, concluding that these systems are most likely collapsing for the first time. Our results strongly suggest that, unlike our current optically selected sample, previous X-ray selected group samples represented a biased picture of the group population. This underlines the necessity of a study of this kind, if one is to reach an unbiased census of the properties of galaxy groups and the distribution of baryons in the Universe.

Key words: galaxies: clusters: general – galaxies: distances and redshifts – X-rays: galaxies – X-rays: galaxies: clusters

1 INTRODUCTION

In hierarchical theories of structure formation, structures of progressively increasing size separate out from the Hubble expansion, recollapse and virialise. Groups of galaxies are the characteristic structures which have formed by the present epoch, and are believed to contain the bulk of the matter in the Universe (Fukugita, Hogan & Peebles 1998). As such, an understanding of the Universe requires an understanding of galaxy groups.

The depth of the potential wells of groups is similar to that of individual galaxies, and galaxy velocities within groups are only a few hundred km s⁻¹. Under these circumstances, galaxies can interact strongly with one another, and with the group potential (e.g. Sérsic 1974; Menon 1992; Verdes-Montenegro et al. 1998;

Mendes de Oliveira et al. 2003; Miles et al. 2004). Hence, not only are groups the most common environment for galaxies, but they provide an environment which has a strong effect on galaxy properties, and which is itself evolving, as groups collapse, virialise and grow through mergers and accretion.

Despite the crucial role played by groups in cosmic structure formation and evolution, they have received relatively little attention compared to larger clusters. This is at least partly due to the fact that typical groups may contain only a handful of bright galaxies in their inner regions. In optical data, groups are therefore often difficult to detect with confidence in projection. X-ray emission from a hot intragroup medium (IGM) provides a much more reliable method of detecting the potential well of a virialised group. Some earlier works based on pointed *ROSAT* X-ray observations utilized this to study the global properties of groups and those of their mem-

* E-mail: jesper@star.sr.bham.ac.uk

ber galaxies in a coherent manner (Mulchaey et al. 1996; Mulchaey & Zabludoff 1998; Zabludoff & Mulchaey 1998; Helsdon & Ponman 2000, 2003; Osmond & Ponman 2004). However, although care had been taken to include groups spanning a wide range of properties, as in the study of Osmond & Ponman (2004), from a statistical viewpoint these works all suffered from the fact that *ROSAT* only targeted a heterogeneous sample of hand-picked groups.

X-ray investigations of optically selected group samples include those of Mahdavi et al. (1997), and later Mahdavi et al. (2000), who invoked data from the *ROSAT* All-Sky Survey (RASS) to study a redshift-selected, unbiased sample of groups in X-rays. However, no detailed information on the galaxy dynamics within these groups was extracted. Burns et al. (1996) also employed RASS data to investigate the X-ray properties of a sample of groups, drawn from the optically selected and statistically complete poor cluster catalogue of Ledlow et al. (1996) and White et al. (1999). This work furthermore included a detailed investigation of the galaxy dynamics within the groups, though the systems were originally selected by photometric enhancements and were not based on velocity information. RASS data also formed the basis for the search for X-ray gas in the optically selected Hickson (1982) catalogue of groups conducted by Ebeling, Voges & Böhringer (1994), a work later augmented by Ponman et al. (1996), who included pointed *ROSAT* data. Even in the latter study, however, the majority (roughly two-thirds) of the groups only had RASS coverage. Due to the shallow RASS exposures of typically a few hundred seconds, the X-ray properties of groups with $L_X \lesssim 10^{42} \text{ erg}^{-1}$ could generally not be investigated in these studies. Moreover, in many cases the data only allowed for a detection of hot intragroup gas, whereas no detailed characterization of gas properties could be carried out. A further concern for RASS-based results for the diffuse X-ray luminosity L_X from groups is the potential danger of contamination from active galactic nuclei due to the broad point spread function (PSF) of the *ROSAT* PSPC at large off-axis angles.

With the exception of dedicated large-scale structure surveys (e.g., Pierre et al. 2004), more recent observations with *XMM-Newton* and *Chandra* have largely been targeting groups already studied by *ROSAT* in pointed observations or serendipitously detected in X-rays as part of the RASS. It is not clear to what extent these groups, most of which are X-ray selected, can be seen as representative of the overall group population at low redshift. Studies of clusters of galaxies indicate that X-ray selection could incorporate a serious bias, with X-ray and optically selected samples showing highly disparate X-ray properties and in some cases (Donahue et al. 2002) being largely non-overlapping. Gilbank et al. (2004) found that a significant fraction of optically selected clusters do not have a clear X-ray counterpart in *ROSAT* data, even though the physical reality of the X-ray faint systems were confirmed by spectroscopic follow-up. A similar conclusion, although based on optical multi-colour imaging rather than spectroscopy, was reached by Barkhouse et al. (2006) using *Chandra* data. The optically selected high-redshift clusters of Lubin, Mulchaey & Postman (2004) were found to be X-ray underluminous for their velocity dispersion σ_v , deviating from the L_X - σ_v relation derived for rich, nearby X-ray

clusters. A similar result was shown for colour-selected clusters by Hicks et al. (2004), while Popesso et al. (2006) found that a subset of their Abell clusters were X-ray underluminous with respect to their virial mass. These results clearly suggest that X-ray selection could provide a biased picture of the cluster population, and there is little reason to assert that the situation for groups should be significantly different. Given the lower X-ray luminosities of groups, such a bias is likely to be even stronger for these systems.

As a consequence of the fact that most X-ray studies of groups have either been concentrating on X-ray selected targets picked from a variety of different group catalogues, or have employed the shallow RASS data to investigate group X-ray emission, we currently have no *unbiased* census of the properties of hot gas and their relation to the dynamics of galaxies within galaxy groups. The advent of large redshift surveys, coupled with the high sensitivity, spatial resolution, and spectral capability of *XMM-Newton* and *Chandra*, has made it possible to remedy this situation. Groups can be selected in redshift space, the properties of any hot IGM can be assessed using deep X-ray data, and group dynamics can be studied with multi-slit spectrographs. We have launched a project to take advantage of this situation, by targeting a statistically representative sample of groups with both *XMM-Newton* and the IMACS multi-object camera and spectrograph (Bigelow & Dressler 2003), installed on the 6.5-m Baade/Magellan telescope at Las Campanas.

The primary aim of the *XI* Project is to understand the nature and evolution of the galaxy group population, and to study the way in which the properties of groups are related to those of their member galaxies. By performing a sensitive test for the presence of any hot IGM in the selected groups, one of the key outcomes of this project will be a reliable estimate of the fraction of optically selected groups which actually contain a hot IGM. Another issue to be addressed is whether the properties of any hot X-ray gas can be used as an evolutionary tracer of the dynamical state of a group. The thrust of the present paper is to provide an initial attack on these questions, using the results obtained for the first four groups observed by *XMM* as part of the project. The large collecting area and field of view of *XMM* makes it the ideal X-ray instrument for this study. IMACS has a field of view perfectly matched to that of *XMM* (~ 30 arcmin in both cases), and allows us to obtain several hundred spectra over this entire field in a single exposure, down to $M_B \approx -15$ at the selected sample redshift of $z \approx 0.06$.

We assume $\Omega_m = 0.3$, $\Omega_\Lambda = 0.7$, and a Hubble constant of $H_0 = 70 \text{ km s}^{-1} \text{ Mpc}$. The virial radius r_{vir} of each group can then be identified with r_{100} , the radius enclosing a mean density of 100 times the critical density ρ_c (Eke, Cole & Frenk 1996). If the dark matter density of the groups follows an 'NFW' profile (Navarro, Frenk & White 1995) with concentration parameters in the plausible range $c = 5 - 20$ (Bullock et al. 2001), we then have $r_{500} \approx 0.5r_{\text{vir}}$. In the adopted cosmology, the characteristic redshift of our sample of $z = 0.06$ corresponds to a luminosity distance $D \approx 275 \text{ Mpc}$, and 1 arcmin to $\approx 70 \text{ kpc}$.

2 GROUP SAMPLE SELECTION

A redshift-selected sample provides the best basis for a study of this type. X-ray selection is impractical, due to the lack of wide-area high-sensitivity data, and would in any case fail to detect groups which are collapsing but do not yet have virialised cores. We therefore selected our sample from the catalogue of 2209 groups derived by Merchán & Zandivarez (2002, hereafter MZ) from a friends-of-friends (FOF) clustering analysis (optimised by reference to cosmological simulations) on the first ('100-K') data release from the 2dF Galaxy Redshift Survey (Colless et al. 2001).

From this large group catalogue, we selected a sample of 25 systems which satisfied the following additional criteria: (i) Redshift $z = 0.060 - 0.063$: This narrow slice puts all groups on an equal observational footing at a redshift where the characteristic radius r_{200} of groups of ~ 1 Mpc corresponds to 13 arcmin and so is well matched to both the *XMM* and IMACS fields of view. Using a narrow redshift interval further has the advantage of circumventing a typical problem associated with FOF-catalogues, namely that the FOF linking length grows with z , implying that the properties of FOF-selected groups may vary systematically with redshift. (ii) Velocity dispersion $\sigma_v < 500$ km s $^{-1}$: Limiting our study to poor systems, which are the most common (containing more than half of all galaxies, see Tully 1987 and Eke et al. 2004) and provide the environment in which dynamical evolution is most rapid, and the dispersion in observed properties is greatest. (iii) Number of spectroscopically confirmed 2dF member galaxies $N_{\text{gal}} \geq 5$: Reducing the danger of including groups which are not real physical associations, by allowing only systems which incorporate at least five 2dF galaxies. N -body simulations show that FOF-groups with $N_{\text{gal}} \geq 5$ almost always correspond to gravitationally bound structures rather than being unbound density fluctuations (e.g., Ramella, Pisani & Geller 1997). (iv) Redshift completeness: We avoid the edges of the 2dF survey area, and regions with poor completeness in the 100-K data release.

Within these constraints, we selected our sample of 25 groups entirely at random. Since our aim is to explore the full population of optically selected systems, we deliberately did not attempt to apply any further constraints of regularity, optical luminosity or dynamical status. Hence our sample contains groups spanning a wide range of properties, subject to having a number density contrast $\delta\rho/\langle\rho\rangle \geq 80$ with respect to the mean galaxy number density $\langle\rho\rangle$, which distinguishes them in the FOF analysis of MZ. To illustrate this diversity in group properties, Fig. 1 shows the distribution of the full sample in the $(r_{\text{vir}}, \sigma_v)$ -plane, with virial radii from Merchán & Zandivarez (2002) based on the projected distribution of galaxies. Highlighted are the four groups targeted for the initial study described in this paper. Basic optical properties of these four groups are provided in Table 1. Note that the subsample studied here includes the two groups with the largest values of σ_v in the full XI sample, and that, within the constraints imposed by our selection criteria, the XI sample covers most of the available parameter space. Also note that, despite the fact that some of the groups are rather compact as judged from the MZ virial radius, we find that none of the XI groups would satisfy the compact group criteria introduced by Hickson (1982). This

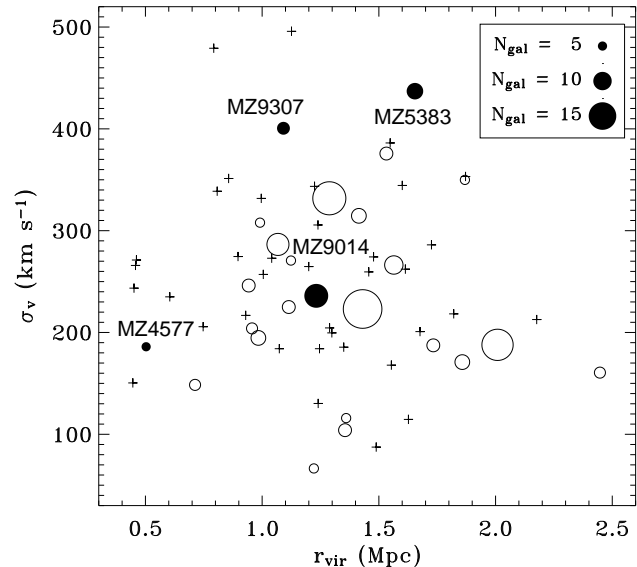


Figure 1. Virial radii and velocity dispersions of all groups satisfying our selection criteria. Groups studied in this paper are marked by filled circles, with the remaining systems in the XI sample shown as empty circles. For the XI groups, the size of each symbol is proportional to the number of member galaxies in each group, as derived by MZ. Velocities have been updated where new IMACS values are available. Remaining groups, meeting our selection criteria but not included in the XI sample, are marked by small crosses.

is in all cases because they fail to meet the compactness criterion $\mu_R < 26.0$, where μ_R is the total R -band magnitude per arcsec 2 of the galaxies within 3 mag of the brightest one, averaged over the (circular) angular extent of the subgroup defined by these galaxies.

Since we initiated the XI project, the 2dF Galaxy Redshift Survey has been completed, and a clustering analysis similar to that of MZ has been carried out on the full catalogue¹, resulting in the 2PIGG group catalogue (Eke et al. 2004). For groups with $N_{\text{gal}} \geq 4$, Eke et al. (2004) find excellent agreement with MZ regarding catalogue-averaged group redshift and velocity dispersion, and the fraction of galaxies grouped. To test for the presence of significant differences in properties between groups specifically fulfilling our selection criteria in the two catalogues, we selected from both of these all groups within the richness range $N_{\text{gal}} = 5 - 24$ occupied by the XI groups in the MZ catalogue, and a three-dimensional velocity dispersion $\sigma < 500$ km/s. To obtain sufficient statistics for a useful comparison, we adopted a wider redshift range $0.04 < z < 0.08$ on either side of the XI group redshifts.

The histograms plotted in Fig. 2 show the resulting distributions of number of member galaxies and velocity dispersion of the 899 2PIGG groups (solid line) and 402 MZ groups (dotted line) that were found in this parameter range. The ratio of the number of groups extracted from the two catalogues, 2.24, is very similar to that of the total number

¹ Available at <http://www.mso.anu.edu.au/2dFGRS/>

Table 1. Basic group properties, including number of confirmed member galaxies N_{gal} , mean recession velocities $\langle v \rangle$, velocity dispersions σ_v , and virial radii r_{vir} from MZ. (*) = updated values from IMACS.

Group	RA (J2000)	Dec (J2000)	N_{gal}	$\langle v \rangle$ (km s $^{-1}$)	σ_v (km s $^{-1}$)	r_{vir} (Mpc)
MZ 4577	11 32 30.79	−04 00 00.8	13 (*)	18614 (*)	186^{+136}_{-28} (*)	$0.50 \approx 7$ arcmin
MZ 5383	12 34 52.83	−03 35 54.3	23 (*)	18120 (*)	437^{+92}_{-43} (*)	$1.65 \approx 23$ arcmin
MZ 9014	00 37 48.12	−27 30 29.1	22 (*)	18239 (*)	236^{+80}_{-45} (*)	$1.23 \approx 17$ arcmin
MZ 9307	00 40 48.64	−27 27 06.1	7	18252	401	$1.09 \approx 15$ arcmin

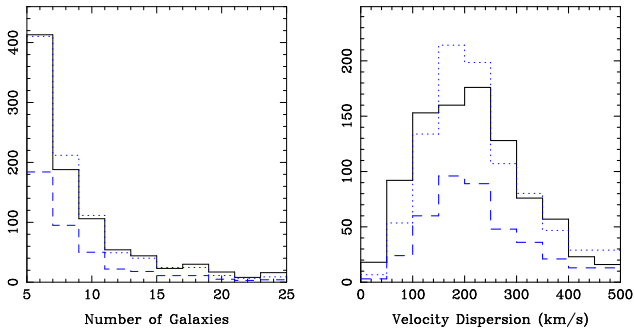


Figure 2. Histograms showing the number of groups versus N_{gal} (left) and σ_v (right) for groups fulfilling our selection criteria in the full 2PIGG group catalogue (solid lines) and the MZ catalogue (dashed lines). The dotted lines represent the MZ subsample scaled to the number of groups in the 2PIGG subsample.

of galaxies in the catalogues. For ease of comparison, the histograms also show the MZ sample scaled by 2.24. The resulting richness histograms for the 2PIGG and (scaled) MZ samples are seen to be almost identical. From a Kolmogorov–Smirnov (K–S) test, the probability that these two samples are significantly different is $P = 3 \times 10^{-7}$. The velocity dispersion histograms peak at roughly the same location, though there is some detailed difference in the structure of the peaks, possibly related to the difference in methods of calculating σ_v between the two catalogues. From a K–S test, the probability that these two samples are significantly different is only $P = 0.044$ however, so we conclude that the 2PIGG and MZ subsamples satisfying our selection criteria are not significantly different.

3 OBSERVATIONS AND ANALYSIS

3.1 Optical data

To obtain photometry, colours, and morphologies of galaxies in the group fields, and to identify candidates for spectroscopic follow-up, images of all groups in the Bessel *BVR* filters were obtained with the 2048×2048 pixel Wide Field Reimaging CCD (WFCCD) on the 100-inch du Pont telescope at Las Campanas. The field of view of 25 arcmin gives a plate scale of 0.77 arcsec pixel $^{-1}$. Twelve dithered exposures were taken for each group and filter, with typical integration times for a group totalling 24 min in *V* and *R* and 60 min in *B*. Images of each group were median-combined and processed using standard IRAF packages, with domeflats used to flatfield the images. Objects were identified using the

SEXTRACTOR package (Bertin & Arnouts 1996), and detections were checked visually. Objects with SEXTRACTOR’s stellarity index > 0.9 were deemed to be definitely stellar and therefore not subject to further analysis. All objects with full-width at half maximum less than the PSF were discarded as noise. A fixed aperture, set to be slightly greater than the seeing, was used to obtain magnitudes in all filters. Objects in different filters were matched, and aperture magnitudes were subtracted to derive colours.

Multi-object spectroscopy of galaxies in the group fields was performed with the IMACS spectrograph on the Baade/Magellan telescope, using short (f/2) camera mode with a grism of 300 lines mm $^{-1}$, giving a wavelength range of 3900–10000 Å and a dispersion of 1.34 Å pixel $^{-1}$. Typical exposure times were 2 hours for each slit mask. Spectroscopic candidates were selected from galaxy lists generated from the *R*-band images taken at the du Pont telescope. Priority was given to the brightest objects in each field, and colour information was not used to select objects. The IMACS data were reduced using a set of programs developed by A. Oemler. First, overscan regions of the CCD chips were used to estimate and subtract the bias level from each frame. Domeflat exposures were then used to flatfield the data. Sky subtraction was performed using the procedure described in Kelson (2003). Finally, wavelength calibrations were determined for each spectrum from exposures of a He-Ne-Ar lamp.

At present we have spectroscopic coverage of 17 of the 25 groups, including three of the four systems discussed here, MZ 4577, 5383 and 9014. Galaxy velocities in these groups were measured by cross-correlating the spectra with galaxy templates as described in Zabludoff & Mulchaey (1998). Typical errors from the template fitting were $\delta v \approx 50$ km s $^{-1}$. From a list of objects with velocities within 2000 km s $^{-1}$ of the group redshift, we determined group membership and velocity dispersion σ_v by using the bi-weight estimator of σ_v (Beers, Flynn & Gebhardt 1990) to iteratively discard 3σ outliers from the group. The 1σ errors on the resulting velocity dispersion were estimated from 10,000 bootstrap trials, as described in Beers et al. (1990).

3.2 X-ray data

The four groups discussed in this paper were all observed by *XMM-Newton* for the nominal exposure time of ~ 20 ks chosen for the *XI* Project. This value is mainly driven by the need to robustly test for the existence of a hot IGM even in groups with X-ray luminosities among the lowest known, $L_X \lesssim 10^{41}$ erg s $^{-1}$. The *XMM* observation log is presented

Table 2. Summary of *XMM-Newton* observations. Column 3 specifies the frame mode (full frame/extended full frame) and optical blocking filter.

Group	EPIC	Obs. mode	t_{exp} (ks)	N_{H} (10^{20} cm^{-2})
MZ 4577	pn	FF-Thin	2.2	4.08
...	MOS1	FF-Thin	3.8	...
...	MOS2	FF-Thin	3.9	...
MZ 5383	pn	FF-Thin	7.5	2.41
...	MOS1	FF-Thin	10.3	...
...	MOS2	FF-Thin	10.7	...
MZ 9014	pn	FF-Thin	22.3	1.54
...	MOS1	FF-Thin	26.4	...
...	MOS2	FF-Thin	26.6	...
MZ 9307	pn	EFF-Medium	2.7	1.48
...	MOS1	FF-Medium	7.7	...
...	MOS2	FF-Medium	8.9	...

in Table 2 which details the observing modes and cleaned exposure times for each EPIC camera.

The *XMM* data were analysed using XMMAS v6.0, and calibrated event lists were generated with the EMCHAIN and EPCHAIN tasks. Event files were filtered using standard quality flags, while retaining only patterns ≤ 4 for pn and ≤ 12 for MOS. Screening for background flares was first performed in the 10–15 keV band for MOS and 12–14 keV for pn. Following an initial removal of obvious large flares, a 3σ clipping of the resulting lightcurve was applied. Point sources were then identified by combining the results of a sliding-cell search (EBOXDETECT) and a maximum likelihood point spread function fitting (EMLDETECT), both performed in five separate energy bands to span the range 0.3–12 keV. In order to filter out any remaining soft protons in the data, a second lightcurve (3σ) cleaning was then done in the 0.4–10 keV band, within a 9–12 arcmin annulus which excluded the detected point sources. Closed-filter data from the calibration database and blank-sky background data (Read & Ponman 2003) for the appropriate observing mode were filtered similarly to source data, and screened so as to contain only periods with count rates within 1σ from the mean of the source data. All point sources were excised out to at least 25 arcsec in spectral analysis.

To aid the search for diffuse X-ray emission within the groups, smoothed exposure-corrected images were produced, with background maps generated from blank-sky data. We allowed for a differing contribution from the non-vignetted particle background component in source- and blank-sky data by adopting the following approach. First an EPIC mosaic image was smoothed adaptively (3σ – 5σ significance range), and the particle background was subtracted. The latter was estimated from closed-filter data which were scaled to match source data count rates in regions outside the field of view, and smoothed at the same spatial scales as the source data. The resulting photon image includes the X-ray background at the source position. To remove this component, a particle-subtracted blank-sky image was produced in a similar way, and scaled to match 0.3–2 keV source count rates in a point-source-excised 10–12 arcmin annulus assumed to be free of IGM emission. This image was then subtracted from the corresponding source image, and

the result was finally exposure-corrected using a similarly smoothed exposure map.

Resulting 0.3–2 keV images of the region of each group covered by all three EPIC cameras are shown in Fig. 3, along with the position of the optical group centre. Rather than adopting the coordinates derived by MZ for the latter (listed in Table 1), these being just a straight mean of the galaxy positions, we have indicated the luminosity-weighted centre instead, calculated from the updated member lists where relevant. It is immediately apparent from these images that none of the groups resembles the relaxed, X-ray bright systems characteristic of X-ray selected group samples.

Using smoothed and unsmoothed versions of the X-ray maps of Fig. 3 along with the significance maps from the smoothing procedure, we searched for evidence of diffuse emission on at least two scales. As earlier *ROSAT* studies showed that most of the detectable IGM emission in X-ray bright groups is typically concentrated within ~ 200 kpc (Helsdon & Ponman 2000), a natural first step was to look for emission within this region, centred on the optical group centre. However, groups in the early stages of collapse will not yet have virialised cores but could still contain shock-heated X-ray gas distributed on larger scales, so we also searched for hot gas within $0.5r_{\text{vir}}$ (where significantly different from 200 kpc), with virial radii taken from Merchán & Zandivarez (2002). As mentioned in Section 1, this radius is expected to correspond to r_{500} for a virialised group, which is the maximum radius out to which group emission has so far been reliably detected with *XMM* (Rasmussen & Ponman 2004). Characterizing the X-ray properties inside this region also allows for a straightforward comparison to the results of Osmond & Ponman (2004), who derived X-ray luminosities inside r_{500} for their sample of 60 groups, by extrapolating fitted surface brightness profiles out to this radius.

We note that the 10–12 arcmin annulus used to evaluate the local soft X-ray background in the imaging data could in principle contain some IGM emission, despite covering a region beginning at a radius comparable to, or greater than, the adopted value of r_{500} for all four groups. If so, some IGM emission would erroneously be subtracted from the images along with the local X-ray background. However, large amounts of IGM emission beyond r_{500} in these seemingly unrelaxed systems would be a real surprise. Indeed, as will be discussed, we do not detect diffuse emission beyond 10 arcmin from the optical group centre for any of the groups, so a 10–12 arcmin annulus is free of detectable IGM emission in all cases (note that Fig. 3 shows only the region covered completely by all three EPIC cameras, and that the adopted annulus is largely outside this region). To help verify this, a 12–14 arcmin annulus was used for comparison, at the expense of losing some detector area within the field of view, resulting in poorer background statistics. Within the Poisson errors, this did not change the number of detected IGM photons for any of the groups.

For the spectral analysis of extended emission, the background was evaluated by means of the common ‘double-subtraction’ technique (Arnaud et al. 2002), using blank-sky background data from Read & Ponman (2003) for the on-chip background, and a large-radius (10–12 arcmin) annulus for determining the local soft X-ray background. For point sources, surrounding 0.5–1 arcmin annuli in the source data

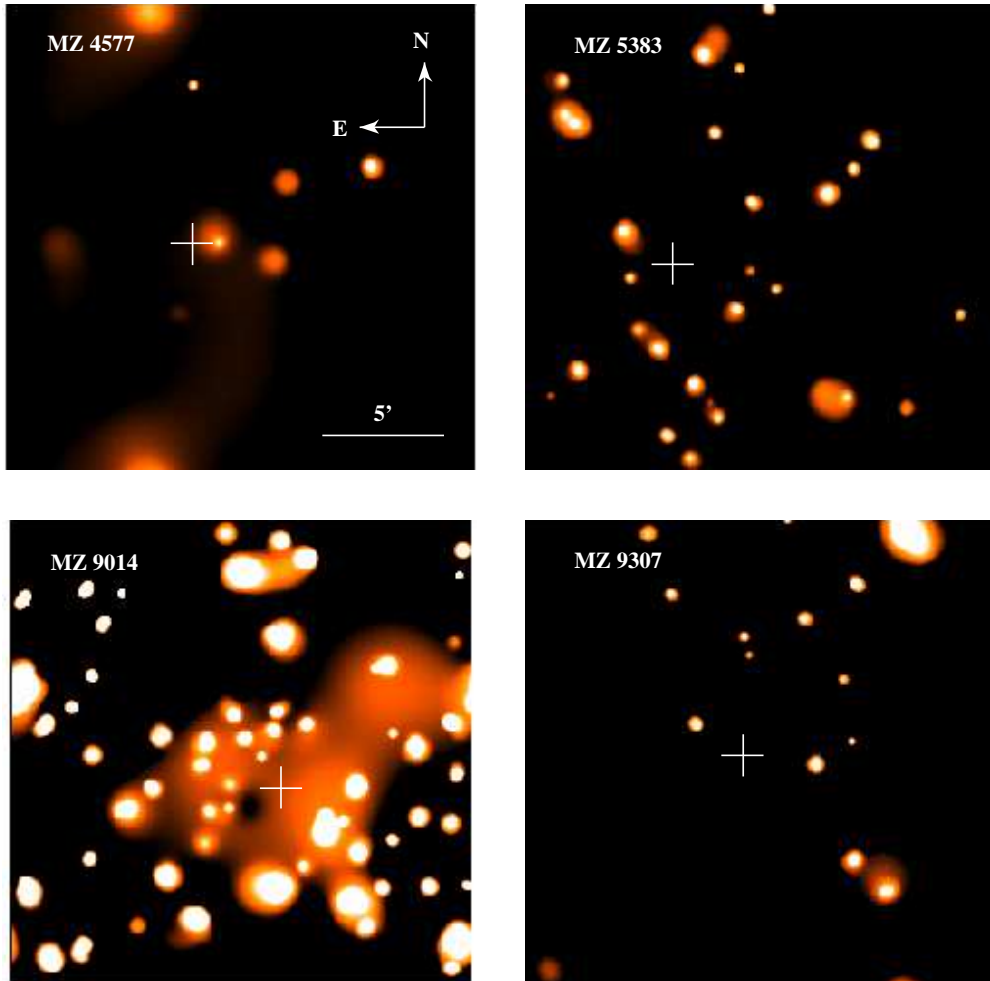


Figure 3. Adaptively smoothed 0.3–2 keV EPIC mosaic images of the central 19×19 arcmin² of each group. A cross marks the position of the luminosity-weighted optical group centre in each case.

were used for background estimates. X-ray spectra were accumulated into bins of at least 20 net counts, and fitted in XSPEC v11.0. Where appropriate, thermal (MEKAL) plasma model fits were used to estimate X-ray luminosities L_X and the mean cooling time $\langle t_{\text{cool}} \rangle \approx 3kT/(\Lambda \langle n_e \rangle)$ of X-ray gas associated with the X-ray detected galaxies and with the IGM itself. Here, $\langle n_e \rangle \sim (EM/V)^{1/2}$ is the mean electron density as inferred from the fitted emission measure EM and the assumed volume V . We have adopted the cooling function $\Lambda(T, Z)$ of Sutherland & Dopita (1993). Where a reliable IGM temperature measurement could not be obtained, T_X was taken from the σ_V – T_X relation of Osmond & Ponman (2004),

$$\log \sigma_V = (1.15 \pm 0.26) \log T_X + 2.60 \pm 0.03, \quad (1)$$

with σ_V in km s^{-1} and T_X in keV. Errors on T were derived from the dispersion of this relation, adding in quadrature the error on σ_V itself. The latter was taken from Table 1 where available, while a 20 per cent error was assumed for MZ 9307. The resulting temperature range, in combination with the conservative assumption of a plasma metallicity

anywhere in the range $0-1 Z_\odot$, was then used to estimate limits to L_X , $\langle n_e \rangle$, $\langle t_{\text{cool}} \rangle$, and total hot gas mass M_{gas} . For X-ray undetected galaxies, only flux and luminosity limits were computed, in all cases assuming a power-law spectrum of photon index $\Gamma = 2$.

4 RESULTS

Optical R -band images of the groups are presented in Fig. 4, along with X-ray contours from Fig. 3. Radial X-ray surface brightness profiles, extracted from the particle-subtracted data with point sources masked out, are shown in Fig. 5. With the aid of these figures, the X-ray and optical results for each group are discussed in detail below.

4.1 MZ 4577

From the analysis of Merchán & Zandivarez (2002), the virial radius of this group is only $r_{\text{vir}} \approx 500$ kpc. This makes it the most compact group in our sample of 25 systems,

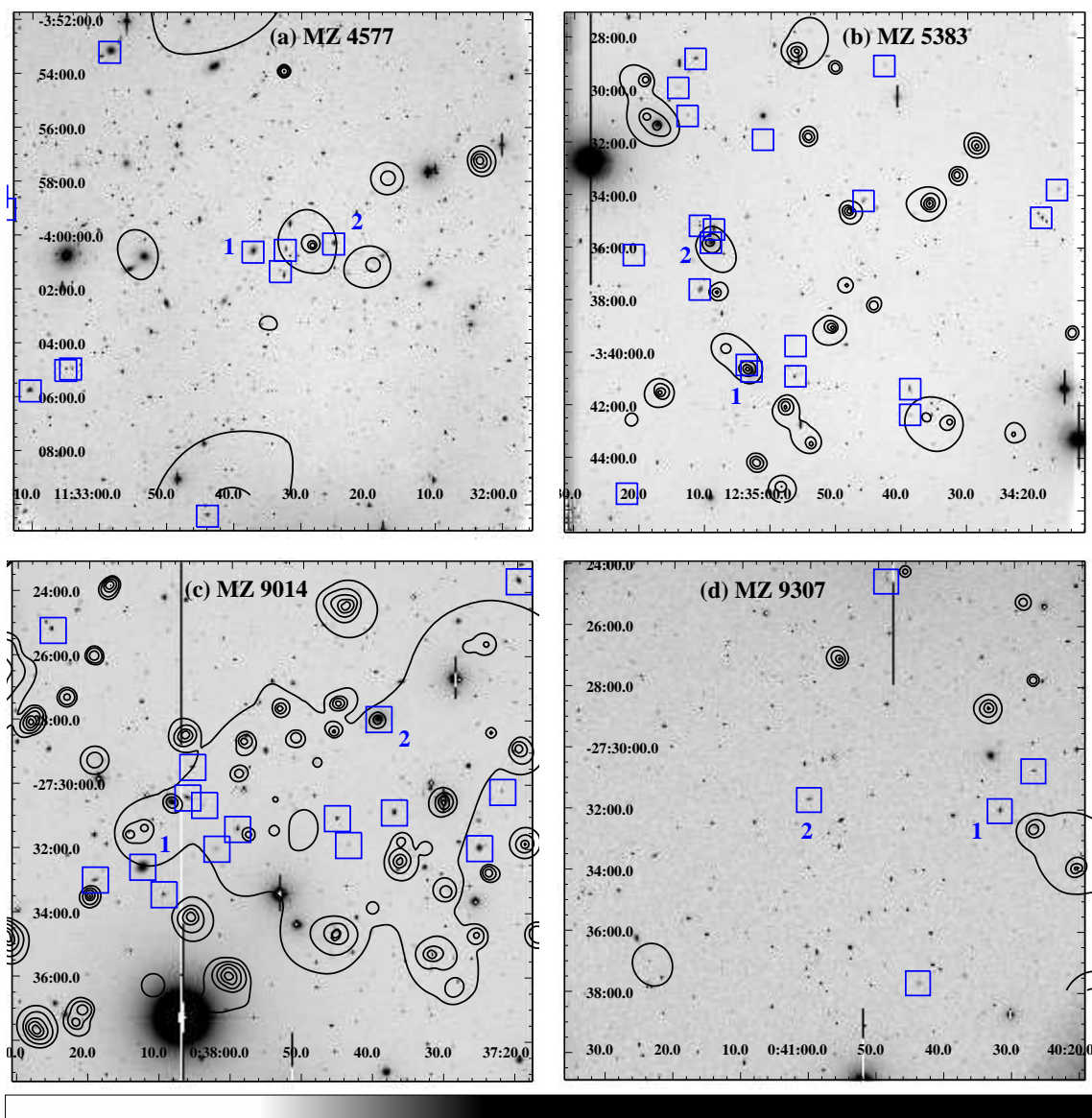


Figure 4. X-ray contours of Fig. 3 overlaid on du Pont *R*-band images of (a) MZ 4577, (b) MZ 5383, (c) MZ 9014, and (d) MZ 9307. X-ray contours are logarithmically spaced over two decades, beginning at (a) 0.5, (b) 1.0, (c) 0.2, and (d) 1.8×10^{-6} photons $\text{s}^{-1} \text{arcsec}^{-2}$, respectively. Confirmed galaxy members are marked by squares, with the first and second-ranked galaxy labelled. For MZ 4577 and MZ 9014, the outermost contour roughly corresponds to the regions inside which X-ray emission is detected at $\geq 3\sigma$ significance.

enabling a search for diffuse X-ray emission inside the full virial radius in our *XMM* observation. As will be discussed in Section 5, the velocity distribution of the 13 spectroscopically identified group galaxies shows a bimodal structure, a fact which underlies the large upper error on our derived value of σ_V listed in Table 1. The updated velocity dispersion from our IMACS data is none the less consistent with the value $\sigma_V = 223 \text{ km s}^{-1}$ listed by MZ on the basis of just five galaxies.

Although a significant fraction of the X-ray exposure was affected by background flares, useful constraints on both diffuse and point-like X-ray emission in the group could still be obtained. We detect seven point sources within the *XMM* field, down to a limiting 0.3–2 keV flux of $\sim 3 \times 10^{-15} \text{ erg cm}^{-2} \text{ s}^{-1}$. None of the confirmed group galaxies

is detected in X-rays, implying a 3σ upper limit to their X-ray luminosities of $L_X \lesssim 2.7 \times 10^{40} \text{ erg s}^{-1}$ inside a 1 arcmin diameter circle. Regarding diffuse X-ray emission in this group, Fig. 3 does not reveal evidence for any clear enhancement in X-ray surface brightness within $r_{\text{vir}} \simeq 7$ arcmin, and the background-subtracted emission level inside r_{vir} is indeed found to be consistent at 1σ with the level outside this region. Nevertheless, there is suggestive evidence for diffuse emission closer to the optical group centre. This is confirmed by the surface brightness profile shown in Fig. 5, centred on the peak of diffuse emission at $(11^{\text{h}}32^{\text{m}}29^{\text{s}}.10, -04^{\circ}00'11''.4)$, which is roughly 50 arcsec east of the luminosity-weighted optical group centre. The profile demonstrates the presence of low-level excess emission inside ~ 50 arcsec from the group centre (note that all X-ray point sources, including

the one seen close to the optical group centre in Figs. 3 and 4, have been masked out when constructing this profile). Quantitatively, a comparison of the source and background X-ray maps described in Section 3.2, indicates the presence of diffuse emission inside $0.5r_{\text{vir}}$ at 2.4σ significance, relative to the background level derived either immediately outside (250–400 kpc) or within a large-radius annulus outside r_{vir} . The smoothing significance map also confirms the presence of marginally significant emission within this central region.

At a level of only ~ 40 net counts, the diffuse emission is too faint to allow any useful spectral analysis. When combined with our errors on σ_v from Table 1, the σ_v - T_X relation for X-ray bright groups, equation (1), would suggest $T = 0.5^{+0.4}_{-0.1}$ keV for the temperature of the IGM in this group. This temperature range would translate into an unabsorbed 0.3–2 keV X-ray luminosity inside $0.5r_{\text{vir}}$ of $2.1 \pm 1.0 \times 10^{41}$ erg s $^{-1}$ at 90 per cent confidence for any subsolar metal abundance $Z \leq Z_{\odot}$. The derived luminosity can be compared to the value of $L_X \approx 9 \times 10^{41}$ erg s $^{-1}$ inside r_{500} suggested by the L_X - σ_v relation of Osmond & Ponman (2004). Thus, the group is X-ray underluminous relative to the expectation from more X-ray bright systems. Under the above assumptions on T and Z , the flux measured inside $0.5r_{\text{vir}}$ would formally imply a mean hot gas density within the range $\langle n_e \rangle = 0.7 - 1.6 \times 10^{-4}$ cm $^{-3}$, a gas mass $1.3 - 3.1 \times 10^{11} M_{\odot}$ (i.e. well below the 10^{12} – $10^{13} M_{\odot}$ typical for X-ray selected groups), and a cooling time in the range 2.4 – 9.7×10^{10} yr. In Table 3, we list some of these results, along with the corresponding constraints obtained for the optically brightest galaxy in the group.

We note that the diffuse emission is unlikely to represent an undetected point source, given its spatial extent and the fact that it is four times brighter than the faintest detected point source in the field. Having no obvious optical counterpart, its centre is displaced from any of the 2dF galaxies by more than 55 arcsec (~ 65 kpc), and so is also unlikely to represent emission from a galactic halo associated with an elliptical within the 2dF redshift range of $z \leq 0.25$. A further argument against association with an elliptical comes from the typical ratio of L_X/L_B of ellipticals (O’Sullivan, Ponman & Collins 2003), which would suggest $L_B \approx 6 \times 10^{10} L_{\odot}$, corresponding to $m_B \approx 15.5$. A galaxy of this optical magnitude would be easily visible in Fig. 4a, where the brightest 2dF galaxy has $m_B = 16.77$.

It is finally worth noting that the luminosity-weighted group centre of MZ 4577 is only 5 arcmin (projected distance ~ 350 kpc) from the centre of the Abell cluster A1308, situated at a redshift of $z = 0.0506$. MZ 4577 could currently be in the process of falling into A1308. However, the radial velocity difference Δv_r between the two structures is roughly $3,600$ km s $^{-1}$, implying $\Delta v_r \gtrsim 4.9\sigma_{\text{cl}}$ for the measured cluster velocity dispersion of $\sigma_{\text{cl}} = 652 \pm 90$ km s $^{-1}$ (De Propris et al. 2002). Even if assuming the systems to be at exactly the same distance and having vanishing transverse peculiar motions, the kinetic energy of the combined system would exceed the gravitational binding energy by at least a factor of 5 (for an assumed cluster mass of $10^{14} M_{\odot}$). It therefore seems unlikely that MZ 4577 is falling into A1308.

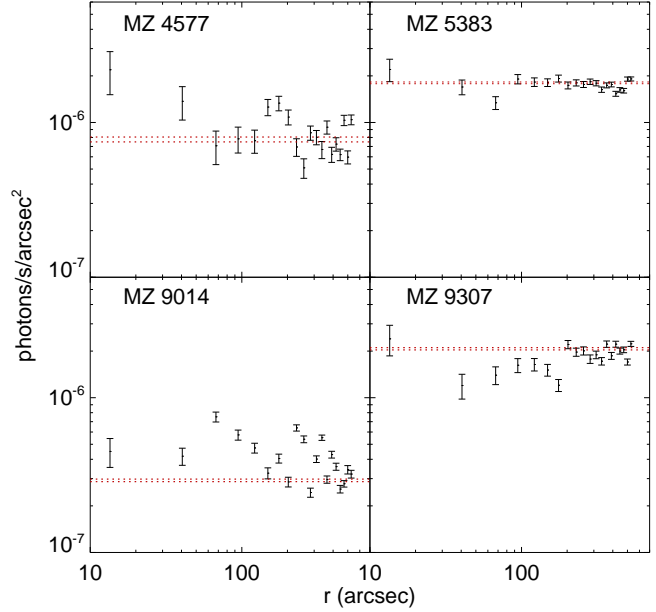


Figure 5. 0.3–2 keV exposure-corrected surface brightness profiles of the diffuse emission in all groups, extracted in 20 equal-size radial bins. Dotted lines show the 1σ errors on the background level as estimated from a surrounding 9–11 arcmin annulus.

4.2 MZ 5383

The distribution of galaxies within this group indicates a relatively large virial radius of 23 arcmin from the MZ analysis. The velocity dispersion is also the largest in the full *XI* sample. Our IMACS results show that one of the 23 spectroscopically confirmed member galaxies is offset from the mean velocity by roughly 1100 km s $^{-1}$ (see Section 5), but eliminating it from the sample would still leave σ_v consistent with the value listed in Table 1. It is not included in the 2dF catalogue and therefore does not contribute to the value $\sigma_v = 417$ km s $^{-1}$ derived by MZ. Despite this relatively large velocity dispersion, the smoothed image in Fig. 3 shows no evidence for a concentration of emission around the luminosity-weighted optical group centre at $(12^{\text{h}}35^{\text{m}}01^{\text{s}}.20, -03^{\circ}37'09''.3)$. The surface brightness profile in Fig. 5, centred on this position due to the lack of any obvious X-ray peak, does not exhibit any systematic radial trend either, nor does it suggest the presence of significant excess emission at any radius. The X-ray maps confirm the absence of emission above the background within both 200 kpc and $0.5r_{\text{vir}}$ from the optical group centre, and we conclude that no emission is detected at 90 per cent confidence outside individual galaxies.

The σ_v - T relation of Osmond & Ponman (2004) would suggest $T = 1.1^{+0.2}_{-0.1}$ keV for the IGM in this group. Our failure to detect any IGM emission then implies a 3σ upper limit to the diffuse 0.3–2 keV luminosity of $L_X < 3.3 \times 10^{41}$ erg s $^{-1}$ inside $0.5r_{\text{vir}}$ for any subsolar metallicity. Again, this can be compared to the expectation $L_X \sim 4 \times 10^{42}$ erg s $^{-1}$ from the L_X - σ_v relation of Osmond & Ponman (2004). Like MZ 4577, this group is thus considerably X-ray fainter than expected from the velocity dispersion of its galaxies. For the assumed limits on T and Z , the luminosity limit im-

plies $\langle n_e \rangle < 3.2 \times 10^{-5} \text{ cm}^{-3}$, $M_{\text{gas}} < 2.2 \times 10^{12} M_{\odot}$, and $\langle t_{\text{cool}} \rangle > 2.9 \times 10^{11} \text{ yr}$ inside $0.5r_{\text{vir}}$.

32 point sources are detected in the field, down to $\sim 3 \times 10^{-15} \text{ erg cm}^{-2} \text{ s}^{-1}$. Emission (inside 0.5 arcmin) at a level of ~ 200 net counts is seen around the first and second-ranked galaxies (both ellipticals). Their spectra suggest thermal plasmas with $T = 0.7 \pm 0.1$ and $0.6 \pm 0.1 \text{ keV}$, and unabsorbed 0.3–2 keV luminosities of $L_X = 2.8 \pm 0.7 \times 10^{41}$ and $2.3 \pm 0.3 \times 10^{41} \text{ erg s}^{-1}$, respectively. Useful constraints on their gas metallicities could not be obtained, so $Z = 0.3 Z_{\odot}$ has been assumed here. Unless counteracted by feedback, this hot gas should be able to cool efficiently within the haloes of the galaxies, having mean cooling times of only $3.2_{-0.3}^{+0.5}$ and $2.5_{-0.1}^{+0.2} \text{ Gyr}$.

4.3 MZ 9014

After flare cleaning, this is the deepest X-ray observation within the present sample. The updated velocity dispersion of the 22 spectroscopically confirmed member galaxies is consistent with the earlier value of $\sigma_v = 240 \text{ km s}^{-1}$ from the MZ catalogue.

As can be discerned from Fig. 3, faint, irregular IGM emission is detected both within 200 kpc and $0.5r_{\text{vir}}$ at more than 3σ significance. This emission is not peaking at the optical group centre which is in fact slightly X-ray fainter than its immediate surroundings (cf. Fig. 3). Exhibiting only ~ 170 net counts, the emission is concentrated along a broad ridge, roughly coinciding with the region occupied by 17 of the 22 member galaxies. Given the absence of a clear X-ray peak and the fact that the brightest group galaxy is located just on the eastern edge of the detected diffuse emission (Fig. 4), the surface brightness profile shown in Fig. 5 has been centred on the diffuse emission centroid at $(00^{\text{h}}37^{\text{m}}40^{\text{s}}.70, -27^{\circ}30'31''.1)$. This was evaluated from an unsmoothed version of Fig. 3 inside a circle enclosing the outermost contour of the 'ridge' seen in Fig. 4. A spectral analysis was also attempted, but a thermal plasma model fit leaves both temperature and abundance unconstrained at 90 per cent confidence. However, within the 1σ errors, the nominal best-fitting value of $T = 0.6 \pm 0.3 \text{ keV}$ is independent of the choice of any subsolar value of Z , and is furthermore in good agreement with the value of $T = 0.6 \pm 0.2 \text{ keV}$ suggested by the σ_v – T relation of Osmond & Ponman (2004).

These results imply a very low IGM luminosity of $L_X = 6 \pm 2 \times 10^{40} \text{ erg s}^{-1}$ inside $0.5r_{\text{vir}}$ for any subsolar metallicity, an order of magnitude below the expectation $L_X \approx 1 \times 10^{42} \text{ erg s}^{-1}$ from both the L_X – σ_v and the L_X – T relation. The derived L_X is lower than that of any system with detectable IGM emission in the *ROSAT*-based sample of Osmond & Ponman (2004), demonstrating the superior ability of *XMM* to detect low surface brightness emission. For the hot gas in the group, we find corresponding ranges of $\langle n_e \rangle = 1.0$ – $3.7 \times 10^{-5} \text{ cm}^{-3}$, $M_{\text{gas}} = 2.8$ – $10.4 \times 10^{11} M_{\odot}$, and $\langle t_{\text{cool}} \rangle$ in the range 1.1 – $6.8 \times 10^{10} \text{ yr}$, for any $Z \leq Z_{\odot}$.

Despite detecting 74 point sources in the field down to $\sim 2 \times 10^{-15} \text{ erg cm}^{-2} \text{ s}^{-1}$, only the optically second-brightest group galaxy, an elliptical, is picked up in X-rays, at a level of ~ 70 net counts. Binning its spectrum into 5 counts per channel, and fitting a $Z = 0.3 Z_{\odot}$ MEKAL model using Cash statistics, yields $T = 0.4 \pm 0.1 \text{ keV}$ and $L_X =$

$4.0_{-0.8}^{+1.5} \times 10^{40} \text{ erg s}^{-1}$, with $\langle t_{\text{cool}} \rangle = 3.8 \pm 0.5 \text{ Gyr}$. The brightest group galaxy, a spiral, is not detected, implying $L_X < 1.7 \times 10^{40} \text{ erg s}^{-1}$.

4.4 MZ 9307

This is another high- σ_v group, along with MZ 5383 the only system in our sample to have $\sigma_v > 400 \text{ km s}^{-1}$ in the original MZ catalogue. The *XMM* observation was performed using the medium optical blocking filter due to a bright star in the field. The presence of significant background flares in the X-ray data did not preclude valuable constraints on the diffuse emission level to be obtained.

No diffuse emission is seen in the X-ray maps, and the surface brightness profile, centred on the luminosity-weighted group centre at $(00^{\text{h}}40^{\text{m}}47^{\text{s}}.11, -27^{\circ}28'18''.8)$, confirms the lack of any enhancement of emission both inside 200 kpc and $0.5r_{\text{vir}}$. The dip in the profile seen around $r \approx 40 \text{ arcsec}$ is present also in the raw data and is thus not an artefact of the background subtraction or exposure correction. The velocity dispersion would suggest $T = 1.0 \pm 0.3 \text{ keV}$ for any hot group gas, and the lack of detectable IGM emission then translates into a 3σ upper limit of $L_X < 5.1 \times 10^{41} \text{ erg s}^{-1}$ for $Z \leq Z_{\odot}$, with $\langle n_e \rangle < 8.0 \times 10^{-5} \text{ cm}^{-3}$, $M_{\text{gas}} < 1.5 \times 10^{12} M_{\odot}$, and $\langle t_{\text{cool}} \rangle > 1.0 \times 10^{11} \text{ yr}$ inside $0.5r_{\text{vir}}$.

We detect 23 point sources in the field, down to a limiting flux of $\sim 2 \times 10^{-15} \text{ erg cm}^{-2} \text{ s}^{-1}$. One of these is an X-ray bright background quasar at $z = 0.170$, just visible to the upper right in Fig. 3. While none of the seven 2dF galaxies in the group is picked up as an X-ray source, our forthcoming IMACS spectroscopy will address whether any optically fainter group galaxies have X-ray counterparts.

5 DISCUSSION

5.1 Comparison to X-ray selected groups

Summarizing the X-ray properties of the hot IGM in the four groups, we find that two groups, MZ 5383 and MZ 9307, show no detectable diffuse emission, whereas MZ 4577 shows some evidence of IGM emission though this is not significant at the 3σ level. Only in one system, MZ 9014, do we detect some irregular emission at $> 3\sigma$ significance. The X-ray luminosity of this system is among the lowest found for any X-ray detected group, and since its hot gas is clearly not in hydrostatic equilibrium, no X-ray mass analysis was attempted.

On the basis of their velocity dispersions, all four groups are remarkably X-ray underluminous with respect to typical X-ray selected groups, as illustrated in Fig. 6. This plot shows the corresponding results from the GEMS sample of Osmond & Ponman (2004), along with several observationally derived L_X – σ_v relations spanning a large range of derived slopes, from $L_X \propto \sigma_v^{1.56}$ (Mahdavi et al. 1997) to $L_X \propto \sigma_v^{4.5}$ (Helsdon & Ponman 2000) (all normalized to our adopted value of H_0). Even when comparing to the combined results from these highly disparate data sets, the XI groups emerge as significantly X-ray underluminous for their velocity dispersions. This is particularly true in light of the

Table 3. X-ray properties of the IGM and the optically brightest group galaxies, down to the brightest X-ray undetected galaxy. Column 3 specifies whether the galaxy is of early (E) or late (S) type.

Group	Rank	E/S?	M_B	T_X (keV)	L_X (10^{40} erg s $^{-1}$)	$\langle t_{\text{cool}} \rangle$ (Gyr)
MZ 4577	IGM	$0.5^{+0.4}_{-0.1}{}^a$	21 ± 10^a	24–97 ^a
...	1	S	−20.45	...	< 2.7	...
MZ 5383	IGM	$1.1^{+0.2}_{-0.1}{}^a$	< 33 ^a	> 290 ^a
...	1	E	−21.13	0.7 ± 0.1	28 ± 7	$3.2^{+0.5}_{-0.3}$
...	2	E	−20.87	0.6 ± 0.1	23 ± 3	$2.5^{+0.2}_{-0.1}$
...	3	S	−20.38	...	< 3.3	...
MZ 9014	IGM	0.6 ± 0.3	6 ± 2	11–68
...	1	S	−20.90	...	< 1.7	...
...	2	E	−20.86	0.4 ± 0.1	$4.0^{+1.5}_{-0.8}$	3.8 ± 0.5
MZ 9307	IGM	1.0 ± 0.3^a	< 51 ^a	> 100 ^a
...	1	E	−18.87	...	< 2.1	...

^a Value derived assuming T_X from the σ_V – T_X relation of Osmond & Ponman (2004), with σ_V from Table 1 (see Section 3 for details).

fact that, apart from the Osmond & Ponman (2004) relation, the X-ray luminosities underlying the L_X – σ_V relations shown in Fig. 6 have generally not been extrapolated to r_{500} . Doing so would raise the normalization of the relations, thus aggravating the discrepancy with respect to the *XI* groups. It is perhaps also surprising that it is the two *XI* groups with the largest values of σ_V that remain undetected in the X-ray. These results indicate already that the full *XI* sample will have properties quite different from the heterogeneous group samples studied in the past, and that these earlier samples provided a biased view of the group population.

Given the importance of this conclusion, it seems worth addressing the robustness of the result shown in Fig. 6, before proceeding to investigate its source of origin. One potential concern is that L_X of our groups has been evaluated inside a fiducial radius of $0.5r_{\text{vir}}$ (assumed roughly equal to r_{500}), for physical consistency and straightforward comparison to the results of Osmond & Ponman (2004). The reliability of the virial radii adopted from MZ for this purpose could be questioned, as these are in some cases based on only five galaxies. This issue will be addressed in more detail when improved membership statistics become available for a larger sample of *XI* groups, but we note for now that the main conclusion – that our four groups are X-ray underluminous for their velocity dispersions – is clearly robust to reasonable changes in r_{vir} .

Another issue is whether the velocity dispersions could be overestimated in our analysis. We tested this for the three groups with available IMACS velocities, by estimating errors on galaxy velocities both from the template fitting code and from the variation in derived redshifts resulting from manually fitting multiple line features. Reassuringly, the resulting values of σ_V were entirely consistent. The argument that σ_V could be artificially boosted by contamination from interlopers could possibly be justified for a single group, but hardly for all four, and certainly not by a factor of 2–3 required to bring MZ 5383, MZ 9014, and MZ 9307 into formal agreement with the L_X – σ_V relation of Osmond & Ponman (2004). For MZ 9307, the velocity dispersion adopted from

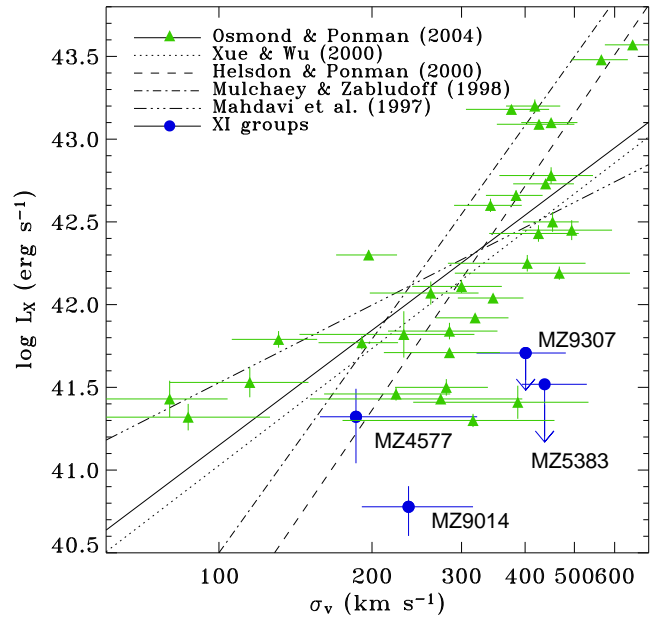


Figure 6. L_X – σ_V relations for X-ray bright groups. Errors on L_X for the *XI* groups are 90 per cent confidence, with downward arrows representing 3σ upper limits. Overplotted are the data points of Osmond & Ponman (2004).

MZ could potentially be unreliable due to the small number of galaxies involved. However, MZ derive σ_V for groups with $N_{\text{gal}} \leq 15$ using the gapper estimator (see e.g. Beers et al. 1990), which should improve robustness in σ_V –estimates for poorly sampled systems. The consistency of the IMACS results for σ_V with the corresponding MZ values for the three other groups also suggests that the adopted velocity dispersion of MZ 9307 cannot be seriously biased.

5.2 Physical state of the IGM

With the robustness of the result shown in Fig. 6 reasonably well established, the question remains how to interpret the lack of significant X-ray emission in our groups, and whether this lack of emission is coupled to their dynamical state. It is most unlikely that the two undetected groups are not gravitationally bound, since (as mentioned in Section 2) only groups with number density contrasts $\delta\rho/\langle\rho\rangle \geq 80$ have been included in the MZ catalogue. This leaves at least three possible explanations for the lack of significant IGM emission in our sample.

(i) The groups could be in the process of collapsing for the first time, in which case the present velocity dispersion could be a poor proxy of the depth of the gravitational potential of the group or the temperature of its X-ray gas. This scenario allows for significant amounts of intragroup gas, which, however, would be more uniformly distributed than in collapsed groups and may not yet have been shock-heated to the virial temperature of the final system. In this case one might also expect to see evidence of dynamical substructure in the galaxy distribution. To investigate this, we plot velocity histograms of the groups in Fig. 7. There is generally some indication, particularly for MZ 5383, of a central gap in the histogram. The result for MZ 4577 also suggests a bimodal velocity distribution, with a subgroup of four galaxies separated from the remaining nine galaxies by $\sim 300 \text{ km s}^{-1}$. These features could be associated with the merging of two subgroups, but there is no convincing evidence that any apparent velocity substructures are localized on the sky in any of the groups. However, given the fairly modest number of galaxies found in each group, it is likely that general conclusions about velocity substructure in these four groups cannot be reached on the basis of individual velocity histograms. To verify this, we confirmed, using the data from Zabludoff & Mulchaey (1998), that apparently virialised systems with a comparable number of confirmed members, such as HCG 42 and NGC 4325, can show velocity histograms with features similar to those seen in Fig. 7.

Potentially, some insight into the dynamics of the groups can still be gained by combining all the velocity measurements. To this end, we constructed a ‘pseudo-group’ containing all confirmed member galaxies, by normalizing the galaxy velocities shown in Fig. 7 to the velocity dispersion of the relevant group. Fig. 8 shows the resulting stacked histogram of the 65 normalized galaxy velocities. It is clear that the central deficit of galaxy velocities persists in this representation. Using a K-S test, we find that the probability that the normalized velocities have been drawn from a Gaussian with unit variance $\sigma_*^2 = [(v - \langle v \rangle)/\sigma_v]^2$, is $P = 0.093$ for all 65 galaxies, decreasing to $P = 0.068$ if including only the 58 galaxies with IMACS velocity measurements. Although still dealing with a relatively small number of galaxies, this result may suggest that the groups, as a class, are still in the process of dynamical relaxation.

A more detailed dynamical analysis of the XI sample will be undertaken when results for the full sample become available. Within the framework of the present analysis, we note that a picture in which the groups are still collapsing also has support from studies of other group samples. These include both purely optical analyses (e.g. Tully

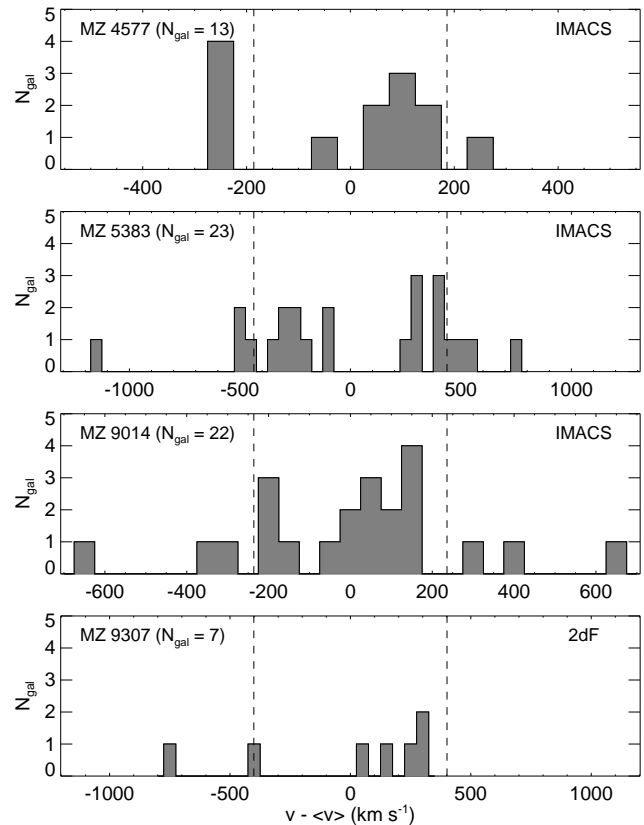


Figure 7. Histogram of galaxy velocities relative to the mean velocity for each group in 50 km s^{-1} bins across the velocity range $\pm 3\sigma_v$. Dashed lines mark σ_v in each case.

1987; Girardi & Giuricin 2000 and references therein) and X-ray/optical comparisons (e.g. Popesso et al. 2006). In particular, Girardi & Giuricin (2000) infer a limiting number density contrast of ~ 70 for their ‘P’ group subsample, comparable to that of the MZ catalogue, and estimate that most of these groups are in the phase of collapse. Popesso et al. (2006) investigated RASS data for a sample of spectroscopically confirmed Abell clusters and found that 50 out of 138 clusters were X-ray underluminous for their optically derived virial mass. Although detecting no obvious optical substructure in their individual X-ray faint clusters, their superior statistics enabled these authors to conclude, on the basis of the position and velocity distributions of the cluster members, that these systems as a class are most likely still collapsing. Further support for ongoing collapse of a considerable fraction of the group population comes from cosmological simulations, which suggest that 30–50 per cent of all groups selected via standard FOF-algorithms could be collapsing for the first time at the present epoch (J. Sommer-Larsen, priv. comm.).

(ii) A second explanation for the general lack of significant X-ray emission in the groups is that the gravitational potentials of these groups are too shallow to heat the intragroup gas to X-ray temperatures. As in scenario (i) above, there could be plenty of intragroup gas, but in this case its temperature would largely remain too low ($\lesssim 10^6 \text{ K}$) to render it detectable in these observations. However, given the high values measured for the velocity dispersions of our

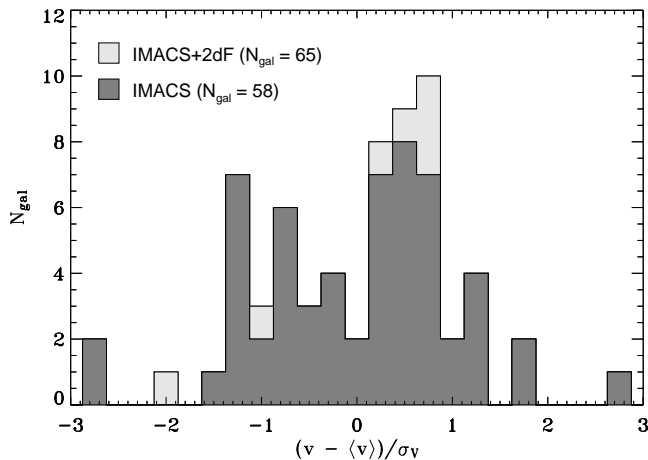


Figure 8. Stacked histogram of all galaxy velocities, measured relative to the mean velocity for each group and normalized to the velocity dispersion of that group. Dark shaded area outlines the histogram for the three groups with IMACS velocities, while the lighter shaded area also includes MZ 9307.

groups, this explanation seems unattractive, and, as has already been discussed, the velocity dispersions of our groups are unlikely to be substantially overestimated. The fact that we *do* detect hot gas in two of the groups also suggests that this scenario cannot offer an exhaustive explanation, even if assuming that the measured velocity dispersions are poor proxies of the total group mass. The long mean cooling times derived for the X-ray detected gas indicate that the gas is emitting inefficiently in the X-ray band due to its density, rather than temperature, being surprisingly low. The fact that MZ 9014 is underluminous relative to the expectation from the L_X - T relation but is consistent with the σ_v - T relation (cf. Section 4.3), seems to support this interpretation.

(iii) Alternatively, the groups could be X-ray faint because many collapsed groups simply contain very little intragroup gas. Our unbiased selection could thus be picking up such systems because they are more numerous than X-ray bright groups. One mechanism which could give rise to this situation is strong galactic feedback ejecting a significant fraction of the original IGM from the group potential. However, that would leave the challenge of explaining why feedback would be so much stronger in some groups as to reduce the X-ray detectable hot gas mass by 1–2 orders of magnitude relative to other systems with potential wells of similar depth. Moreover, since the formation of elliptical galaxies is expected to generate more feedback than that of spirals (Arnaud et al. 1992), strong group-wide feedback would probably require a galaxy population with a low spiral fraction $f_{\text{sp}} = N_{\text{sp}}/N_{\text{gal}}$. If tentatively identifying those 2dF group galaxies with values of the spectral type parameter $\eta > -1.4$ as spirals (see Madgwick et al. 2002), then the mean spiral fraction of our four groups is ~ 65 per cent. Such a large value of f_{sp} may not be easily reconciled with the notion that galactic feedback has ejected much of the IGM from the groups.

We note that Mahdavi et al. (2000) detected X-ray emission in RASS data from only 42 out of a statistically complete sample of 260 groups, suggesting that ~ 75 per cent of their groups do not contain a hot IGM.

However, due to the very shallow RASS exposures, these authors could not study X-ray emission from groups with $L_X \lesssim 10^{42}$ erg s^{-1} , which would be expected to be more common. In fact, based on the expectation from X-ray bright groups, more than half of the 25 *XI* groups are expected to show X-ray emission around or below this limit (cf. Figs. 1 and 6). Until a larger sample of such groups has been studied using more sensitive X-ray data, it seems premature to accept scenario (iii) without considering viable alternatives.

In summary, we cannot at this stage exclude the possibility that the surprisingly low diffuse X-ray luminosity of our groups is due to any IGM being either largely absent or too cold to produce copious X-ray emission. In order to help constrain the *total* gas content of the *XI* groups, we have commenced a programme of HI imaging of the groups using the Giant Metrewave Radio Telescope. When HI results for a significant number of groups become available, we will be in a better position to assess the validity of scenarios ii) and iii) above. Until then, we find the idea that the groups could still be in the process of virialisation more attractive. In contrast to the other scenarios discussed, this explanation draws support from both cosmological simulations and other observational group studies, without facing any immediate challenges.

We note that the morphological composition and the likely dynamical status of these groups suggest an analogy to the Local Group (LG) of galaxies, which consists of three spirals brighter than $M_V \sim -19$, with a varied assortment of early and late-type dwarfs, and is collapsing for the first time. Although having a low velocity dispersion of $\sigma_v \sim 100$ km s^{-1} , comparable to those of the lowest- σ_v groups in the *XI* sample (Fig. 1), the total LG mass of $\sim 2 \times 10^{12} M_\odot$ (e.g. van den Bergh 1999) suggests a mass overdensity with respect to the critical density of ~ 45 , within the region occupied by the Milky Way and M31 subgroups. The equivalent galaxy number density contrast in the adopted cosmology of $\delta\rho/\langle\rho\rangle \sim 150$ suggests that the LG would in fact meet the overdensity criterion for inclusion in the MZ catalogue. Though no X-ray emitting hot IGM has yet been detected in the LG, which is unlikely to have a diffuse X-ray luminosity of more than a few times 10^{40} erg s^{-1} (Rasmussen & Pedersen 2001), recent detections of zero-redshift OVI and OVII absorption lines in *FUSE* and *Chandra* observations of quasars suggest the presence of an LG intergalactic medium of electron density $\sim 5 \times 10^{-6}$ cm^{-3} and temperature $T \lesssim 10^6$ K (e.g. Nicastro et al. 2003). This is consistent with the low fluxes we observe for our groups. Our HI studies of the *XI* groups will help us compare their cold gas content with that of the LG.

5.3 Properties of group galaxies

As will be described in more detail in a subsequent paper, a substantial fraction of the *XI* group members are found from our IMACS spectroscopy to be emission-line galaxies. In particular, strong optical emission lines are found in roughly half of the confirmed member galaxies in the three groups with IMACS data discussed here. Hence, star-forming galaxies and active galactic nuclei are seen in all of these groups. Given this, it is perhaps surprising that out of a total of 58 confirmed group galaxies, we detect X-ray

emission above a few times 10^{40} erg s^{-1} in only three of them (cf. Tables 1 and 3). These three galaxies are all ellipticals, displaying no evidence for significant optical emission lines. Their X-ray luminosities are fairly typical of moderately X-ray bright ellipticals, and their measured luminosities and temperatures compare well to the expectations from the L_X - T relation derived for ellipticals by O’Sullivan et al. (2003). The galaxies that show AGN-like optical emission in our groups must have X-ray emission below our detection limit of $\sim 2 - 3 \times 10^{40}$ erg s^{-1} , and their nuclei could be related to the class of low-luminosity AGN seen in some nearby galaxies (see, e.g., Terashima et al. 2002).

From an optically selected sample of groups having pointed *ROSAT* PSPC coverage, Zabludoff & Mulchaey (1998) found that groups with detectable X-ray emission typically have a bright ($M_B \lesssim M_B^* - 1 \approx -21.4$) elliptical at the centre of the X-ray emission. In addition to the unexpectedly faint IGM emission of the four XI groups studied here, another potential difference between these and more X-ray luminous systems is therefore that none of our groups hosts a dominant central elliptical galaxy. In two of the groups, including the X-ray detected MZ 9014, the optically most luminous galaxy is in fact a spiral. None of the ellipticals is 1 mag brighter than M_B^* , and we note in particular that the brightest 2dF galaxy in MZ 9307 is ~ 1.5 mag fainter than M_B^* . The absence of a dominant elliptical in the groups also seems to support the hypothesis that the groups are still collapsing, since such galaxies are probably formed via mergers in dense environments.

We should also note, though, that the two X-ray detected groups, MZ 4577 and MZ 9014, are not the only systems known to show diffuse intragroup X-ray emission which is not peaking on a central, bright early-type galaxy. Other examples include the spiral-dominated Hickson compact groups HCG 16 (Dos Santos & Mamon 1999; Belsole et al. 2003), HCG 57 (Fukazawa et al. 2002), and the well-studied HCG 92 (Stephan’s Quintet; Sulentic, Pietsch & Arp 1995; Awaki et al. 1997; Pietsch et al. 1997; Trinchieri et al. 2003, 2005), as well as the early-type dominated HCG 37 (Mulchaey et al. 2003). These groups all exhibit low diffuse X-ray luminosities in the range $\approx 1-5 \times 10^{41}$ erg s^{-1} , comparable to L_X of the X-ray detected XI groups. Systems like the Hickson groups, likely to represent groups close to maximum collapse, are not very common in the nearby Universe, however. For example, we find that only about ~ 1 per cent of the groups in the MZ catalogue (and, as mentioned in Section 2, none of the XI groups) satisfy the Hickson (1982) criteria. Outside Hickson’s catalogue, other examples are NGC 7777 and SHK 202 (Mulchaey et al. 2003). However, the number of such systems in the literature is still very low, placing MZ 4577 and MZ 9014 in an exclusive club. Coupled with the results described in Section 5.1, this is a further indication that the XI project is targeting a class of groups not previously studied in much detail in X-rays.

6 CONCLUSIONS

As part of an ongoing effort to investigate the X-ray and optical properties of a substantial, statistically unbiased, and kinematically selected sample of galaxy groups, for the first time using deep X-ray data, we have performed *XMM-*

Newton observations of the first four groups in this sample. In two of the groups, we detect an X-ray emitting intragroup medium, with luminosities among the lowest found for X-ray detected groups so far. The two other groups observed here remain undetected in the X-ray, and all four groups are found to be X-ray underluminous for their velocity dispersions when compared to expectations from X-ray bright groups. Furthermore, none of the groups hosts a dominant elliptical galaxy at the centre of the X-ray emission. Our results therefore suggest that the nature of the IGM in these optically selected groups may be very different from that seen in standard X-ray selected group samples. The fact that we are finding some of the faintest IGM yet seen in groups in our first four observations clearly demonstrates that the XI Project is exploring new parameter space. It also establishes that the predominantly X-ray selected group samples studied in the past with e.g. *ROSAT* were not representative of the overall group population. In contrast, the unbiased redshift selection employed in the XI Project appears to be targeting a different class of groups not previously studied in much detail.

The low levels of IGM emission in the groups could be an indication that i) the groups are in the process of collapsing for the first time, ii) the gravitational potentials are too shallow for the gas to emit much X-ray emission (i.e. the gas is essentially too cool to produce X-rays), or iii) there is simply little or no intragroup gas. We find the first explanation to be the more attractive, at least until the validity of the other scenarios can be more firmly addressed by subjecting a larger sample of optically selected groups to deep X-ray observations. The idea that many groups are collapsing for the first time at the present epoch is also consistent with expectations from other optical group studies and with results of cosmological simulations.

In contrast to the more well-studied class of X-ray bright groups, the type of groups studied in this paper truly represents the most common galaxy environments in the Universe. Investigating the detailed properties of a larger sample of such groups is therefore crucial if one is to obtain an unbiased understanding of the nature of the group population and a census of the distribution of baryons in the Universe.

ACKNOWLEDGMENTS

We thank Gus Oemler, Dan Kelson, and Greg Walth for their role in developing the IMACS reduction pipeline, Gary Mamon, Andrea Biviano, and Jesper Sommer-Larsen for useful discussions, and the referee for comments which helped improve this paper. JR acknowledges the support of the European Community through a Marie Curie Intra-European Fellowship under contract no. MEIF-CT-2005-011171. JSM acknowledges partial support from NASA grants NNG04GF78G and NNG04GC846.

REFERENCES

- Arnaud M., Rothenflug R., Boulade O., Vigroux L., Vangioni-Flam E., 1992, *A&A*, 254, 49
- Arnaud M. et al., 2002, *A&A*, 390, 27

- Awaki H., Koyama K., Matsumoto H., Tomida H., Tsuru T., Ueno S., 1997, PASJ, 49, 445
- Barkhouse W.A., et al., 2006, ApJ, 645, 955
- Beers T.C., Flynn K., Gebhardt K., 1990, AJ, 100, 32
- Belsole E., Sauvageot J.-L., Ponman T.J., Bourdin H., 2003, A&A, 398, 1
- Bertin E., Arnouts S., 1996, A&AS, 117, 393
- Bigelow B.C., Dressler A.M., 2003, Proc. SPIE, 4841, 1727
- Bullock J.S., Kolatt T.S., Sigad Y., Somerville R.S., Kravtsov A.V., Klypin A.A., Primack J.R., Dekel A., 2001, MNRAS, 321, 559
- Burns J.O., Ledlow M.J., Loken C., Klypin A., Voges W., Bryan G.L., Norman M.L., White R.A., 1996, ApJL, 467, L49
- Colless M. et al., 2001, MNRAS, 328, 1039
- De Propris R. et al., 2002, MNRAS, 329, 87
- Donahue M. et al., 2002, ApJ, 569, 689
- Dos Santos S., Mamon G.A., 1999, A&A, 352, 1
- Ebeling H., Voges W., Böhringer H., 1994, ApJ, 436, 44
- Eke V.R., Cole S., Frenk C.S., 1996, MNRAS, 282, 263
- Eke V.R. et al., 2004, MNRAS, 348, 866
- Fukazawa Y., Kawano N., Ohto A., Mizusawa H., 2002, PASJ, 54, 527
- Fukugita M., Hogan C.J., Peebles P.J.E., 1998, ApJ, 503, 518
- Gilbank, D.G., Bower R.G., Castander F.J., Ziegler B.L., 2004, MNRAS, 348, 551
- Girardi M., Giuricin G., 2000, ApJ, 540, 45
- Helsdon S.F., Ponman, T.J., 2000, MNRAS, 315, 356
- Helsdon S.F., Ponman, T.J., 2003, MNRAS, 340, 485
- Hicks A., Ellingson E., Bautz M., Yee H., Gladders M., Garmire G., 2004, 35th COSPAR Scientific Assembly, 1624
- Hickson P., 1982, ApJ, 255, 382
- Kelson D.D., 2003, PASP, 115, 688
- Ledlow M.J., Loken C., Burns J.O., Hill J.M., White R.A., 1996, AJ, 112, 388
- Lubin L.M., Mulchaey J.S., Postman M., 2004, ApJL, 601, L9
- Madgwick D.S. et al., 2002, MNRAS, 333, 133
- Mahdavi A., Böhringer H., Geller M.J., Ramella M., 1997, ApJ, 483, 68
- Mahdavi A., Böhringer H., Geller M.J., Ramella M., 2000, ApJ, 534, 114
- Mendes de Oliveira C., Amram P., Plana H., Balkowski C., 2003, AJ, 126, 2635
- Menon T.K., 1992, MNRAS, 255, 41
- Merchán M., Zandivarez A., 2002, MNRAS, 335, 216
- Miles T.A., Raychaudhury S., Forbes D.A., Goudfrooij P., Ponman T.J., Kozhurina-Platais V., 2004, MNRAS, 355, 785
- Mulchaey J.S., Zabludoff A.I., 1998, ApJ, 496, 73
- Mulchaey J.S., Davis D.S., Mushotzky R.F., Burstein D., 1996, ApJ, 456, 80
- Mulchaey J.S., Davis D.S., Mushotzky R.F., Burstein D., 2003, ApJS, 145, 39
- Navarro J.F., Frenk C.S., White S.D.M., 1995, MNRAS, 275, 720
- Nicastro F. et al., 2003, Nature, 421, 719
- O'Sullivan E., Ponman T.J., Collins R.S., 2003, MNRAS, 340, 1375
- Osmond J. P. F., Ponman T. J., 2004, MNRAS, 350, 1511
- Pietsch W., Trinchieri G., Arp H., Sulentic J.W., 1997, A&A, 322, 89
- Pierre M. et al., 2004, JCAP, 9, 11
- Ponman T.J., Bourner P.D.J., Ebeling H., Böhringer H., 1996, MNRAS, 283, 690
- Popesso P., Biviano A., Böhringer H., Romaniello M., 2006, A&A, in press (astro-ph/0606191)
- Ramella M., Pisani A., Geller, M.J., 1997, AJ, 113, 483
- Rasmussen J., Pedersen K., 2001, ApJ, 559, 892
- Rasmussen J., Ponman T.J., 2004, MNRAS, 349, 722
- Read A.M., Ponman T.J., 2003, A&A, 409, 395
- Sérsic J.L., 1974, Ap&SS, 28, 365
- Sulentic, J.W., Pietsch W., Arp H., 1995, A&A, 298, 420
- Sutherland R.S., Dopita M.A., 1993, ApJS, 88, 253
- Terashima Y., Iyomoto N., Ho L.C., Ptak A.F., 2002, ApJS, 139, 1
- Trinchieri G., Sulentic J., Breitschwerdt D., Pietsch W., 2003, A&A, 401, 173
- Trinchieri G., Sulentic J., Pietsch W., Breitschwerdt D., 2005, A&A, 444, 697
- Tully, R.B., 1987, ApJ, 321, 280
- van den Bergh S., 1999, A&AR, 9, 273
- Verdes-Montenegro L., Yun M.S., Perea J., del Olmo A., Ho P.T.P., 1998, ApJ, 497, 89
- White R.A., Bliton M., Bhavsar S.P., Bornmann P., Burns J.O., Ledlow M.J., Loken C., 1999, AJ, 118, 2014
- Zabludoff A.I., Mulchaey J.S., 1998, ApJ, 496, 39

This paper has been typeset from a \TeX / \LaTeX file prepared by the author.